Transition Mechanisms for Complex Ordered Phases in Block Copolymer Melts

Damian A. Hajduk,*,† Rong-Ming Ho,‡ Marc A. Hillmyer,§ and Frank S. Bates*

Department of Chemical Engineering and Materials Science, University of Minnesota, Minneapolis, Minnesota 55455

Kristoffer Almdal

Risø National Laboratory, DK-4000 Roskilde, Denmark

Received: September 3, 1997; In Final Form: November 25, 1997

We describe microstructural aspects of phase transitions between the lamellar (L), perforated layer (PL), and gyroid (G) morphologies in diblock copolymer melts. Using small-angle scattering, dynamic mechanical spectroscopy, and transmission electron microscopy, we show that these transformations proceed through the nucleation and growth of the final phase, in contrast to recent calculations that assume evolution from a thermodynamically unstable initial state. Direct L → G transitions are suppressed by the high surface tension associated with L−G grain boundaries; the formation of the metastable PL structure under such conditions reflects the ease with which the L → PL transition can occur, compared to L → G. Similar effects dominate the G → L transition. Mismatches in spacings between epitaxially related lattice planes also influence relaxation kinetics; the P → LG transition rate depends strongly on the relative spacings of the PL [10] and G [211] planes, and the considerable discrepancy between the G [211] and L [10] spacings at the L−G boundary may further retard that transformation. Similar factors have been shown to govern the evolution of amphiphilic systems, supporting geometrically inspired attempts to understand this phase behavior.

Introduction

Despite considerable interest in the equilibrium aspects of diblock copolymer phase behavior, the kinetics of transitions between different microphase-separated morphologies (order−order transitions, or OOTs) have received comparatively little attention. Both experimental[1] and theoretical[2] data indicate that in the vicinity of the order−disorder transition (ODT), phase boundaries acquire significant curvature in the composition (f)−segregation (χN) plane, and the system becomes thermotropic due to the temperature dependence of χ. Far from the ODT, phase boundaries become nearly independent of segregation;[3−9] in this regime, nonequilibrium morphologies can be prepared through casting from a selective solvent and their relaxation can be followed by a variety of techniques.[10,11] Since the relaxation mechanism may dictate the structural perfection of the resulting mesophase, an understanding of these processes has implications for the practical control of copolymer morphology.

If the initial state is thermodynamically unstable, relaxation occurs through the exponential growth of concentration fluctuations, a relatively fast process that might initially result in a poorly ordered morphology. Theoretical calculations often address such unstable states in order to avoid complications related to nucleation and growth, such as determination of the surface tension associated with grain boundaries separating initial and final phase domains. Using a time-dependent Ginzburg−Landau model with a single-wavenumber approximation, Qi and Wang[12−14] analyzed transitions between the lamellar (L), cylindrical (C), and spherical (S) morphologies; the gyroid (G) morphology was not included in the calculations. The hexagonally perforated layer (HPL) phase appeared as a pseudostable morphology during the LC transition; it was shown to consist of two nearly degenerate states, one in which the channels extending through the minority component domain adopt hexagonal in-plane symmetry (hcp-based PL) and one in which they exhibit tetragonal in-plane symmetry (bcc-based PL). Superposition of these states produced the neutron diffraction identified in earlier studies. Shi et al.[15] and Laradji et al.[16,17] have developed a general approach for studying such fluctuations through an expansion about the mean-field solution to the self-consistent field theory for copolymer melts. They predict unstable fluctuation modes for the L and C morphologies and epitaxial relations connecting the L, G, C, and S phases, which are in good agreement with experimental data.[18−21]

To date, however, the (limited) experimental evidence is more consistent with nucleation and growth. Here, thermal fluctuations within the metastable initial phase generate nuclei of the final morphology, which then grow to encompass the sample volume. Prior to completion of the process, the sample consists of coexisting domains of the two morphologies; such coexistence has been observed during the L → C,[18,19] C → L,[18,19] and G → L[22] transitions. Although a comprehensive theoretical description of this behavior has not been presented, Goveas and Milner[23] have examined the growth of the stable morphology in weakly segregated melts consisting of coexisting L and C domains. Studies of the disorder-to-order transition indicate that this mechanism governs microphase separation;[24−29] it is not obvious, however, that it governs order-order transitions as well.

* To whom correspondence should be addressed.
† Current address: Symyx Technologies, 3100 Central Expressway, Santa Clara, CA 95051.
‡ Current address: Department of Chemical Engineering, National Chung Hsing University, Taichung 402, Taiwan, ROC.
§ Current address: Department of Chemistry, University of Minnesota, Minneapolis, MN 55455.

S1089-5647(97)02871-X CCC: $15.00
Published on Web 02/03/1998

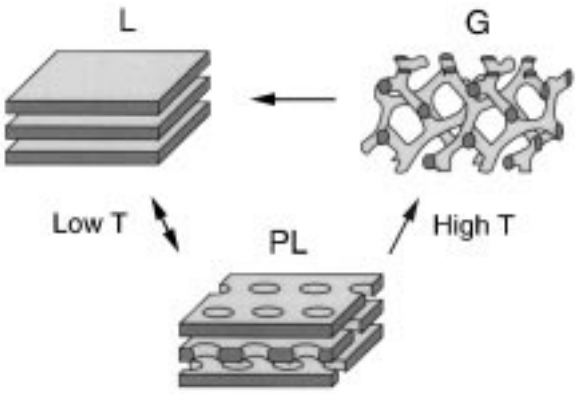

Figure 1. Minority component domains of the lamellar (L), perforated layer (PL), and gyroid (G) morphologies; the surrounding volume is filled with the majority component material. Upon heating, the materials discussed in this paper transform from the L phase, through the (nonequilibrium) PL structure, to the G phase. As indicated by the arrows, the L → PL transition is reversible, while the PL → G and G → L transitions are not.

TABLE 1: Molecular Characteristics

sample name	f [a]	M_n [b]
Polyisoprene−Polystyrene (PS−PI)[35]		
IS−65	0.65	39.5
IS−66	0.66	39.7
Poly(ethylene-*co*-propylene)−Poly(dimethylsiloxane) (PEP−PDMS)[36]		
PEP−PDMS 7	0.64	10.4
Poly(ethylene oxide)−Poly(ethylethylene) (PEO−PEE)[37,38]		
OE−10	0.72	8.7

[a] f is the volume fraction of the block given first in the name for the copolymer and possessing the lower value of R_g2/V, where R_g is the radius of gyration and V is the block volume. [b] M_n is the number-average molecular weight in kg/mol.

Recently, we demonstrated that the hexagonally modulated layer (HML) and hexagonally perforated layer (HPL) morphologies, previously identified as equilibrium structures in a narrow range of compositions separating the L and C phases, are in fact long-lived nonequilibrium morphologies involved in the LG transition.[30] In the HPL phase, the hexagonal in-plane packing of the channels extending through the minority component domains was shown to result from application of a shear field; the unsheared morphology was identified as perforated layers (PL). Here, we examine the mechanics of the L → G transition in order to identify factors governing the formation of the PL structure and its subsequent conversion into the G morphology. Using a combination of small-angle X-ray and neutron scattering, dynamic mechanical spectroscopy, and transmission electron microscopy, we describe the microstructural changes and epitaxial relations associated with the L → PL, PL → G, and G → L transformations (Figure 1). The factors governing these behaviors resemble those previously identified in studies of amphiphilic suspensions,[31−34] suggesting that common geometrical characteristics may play a significant role in determining the transition mechanisms.

Experimental Section

The synthesis and initial morphological characterization of the polymers used in this study have been described in detail elsewhere (see Table 1). Films of IS-65 and IS-66 were prepared by melt pressing of the precipitated copolymer into sheets 0.5 mm thick in a vacuum at 120 °C. Samples of poly(ethylene oxide)−poly(ethylethylene) (PEO−PEE) copolymers were prepared by melt pressing at 50 °C followed by crystallization of the PEO block at room temperature. This resets the sample morphology to a randomly oriented, semicrystalline lamellar phase, minimizing the effect of nonequilibrium morphologies arising from sample preparation. Poly(ethylene-*co*-propylene)−poly(dimethylsiloxane) (PEP−PDMS) copolymers were used as recovered from polymerization.

Viscoelastic characteristics were measured on a Rheometrics RSA-II rheometer using a reciprocating shear sandwich geometry with a sample thickness of 0.5 mm. A nitrogen purge was used to minimize oxidative degeneration at high temperatures. PS−PI samples were cut from films prepared as described above and mounted on the rheometer plates at 80 °C. After the plates were heated to 110 °C under nitrogen, the gap thickness was adjusted to 0.5 mm and the plates were cooled to room temperature in order to remove any excess material. PEO−PEE samples were melted at 50 °C and placed on the rheometer plates. After the gap thickness was adjusted, excess material was removed and the polymer was permitted to recrystallize at 10 °C prior to beginning measurements. Isothermal frequency sweeps measured the elastic (G') and loss (G'') moduli at a constant temperature over frequencies (ω) from 0.1 to 100 rad/s; temperature sweeps monitored $G'(T)$ and $G''(T)$ at frequencies from 0.1 to 1.0 rad/s while scanning at rates from 0.1 to 10 °C/min. Strain amplitudes of 1% were employed unless otherwise indicated.

Small-angle X-ray scattering (SAXS) measurements were conducted on a small-angle beamline constructed at the University of Minnesota. Cu Kα X-rays were generated by a Rigaku RU-200BVH rotating anode X-ray machine equipped with a 0.2 × 2 mm microfocus cathode and Franks mirror optics. Samples were placed inside an evacuated sample chamber and maintained at the appropriate temperature by a pair of heaters mounted on a water-cooled brass block (temperature range 5−260 °C, stability ±0.1 °C). Two-dimensional diffraction images were collected with a multiwire area detector (HI−STAR, Siemens Analytical X-ray Instruments) and corrected for detector response characteristics prior to analysis.

Small-angle neutron scattering (SANS) measurements were conducted on the 12-m Å instrument at Risø National Laboratory in Roskilde, Denmark using $\lambda = 6.0$ Å neutrons ($\Delta\lambda/\lambda = 0.09$) with a sample-to-detector distance of 3.0 m. Simultaneous rheological and scattering measurements were obtained on a Rheometrics RSA-II rheometer that was mounted in the neutron beam. The instrument utilized a reciprocating shear sandwich geometry in which the incident radiation was parallel to the shear gradient direction. Windows in the oven surrounding the (aluminum) test fixtures permitted passage of the beam through the specimen. Sample thicknesses of 0.3 or 0.5 mm were used, depending on the shear amplitude desired; sample preparation methods were identical with those described above for rheological studies.

Transmission electron microscopy (TEM) was conducted on a JEOL JEM-1210 electron microscope operated at 120 kV. Selected polystyrene−polyisoprene copolymers (both unsheared and shear-oriented) were quenched from high temperatures into ice water or liquid nitrogen to vitrify the polystyrene block and preserve the high-temperature morphology. Sections of 500−1000 Å in thickness were cut from the bulk specimen using a Reichert Ultracut S microtome equipped with a Reichert FCS cryochamber and a diamond knife and picked up on copper grids. Polyisoprene (majority component) domains were stained

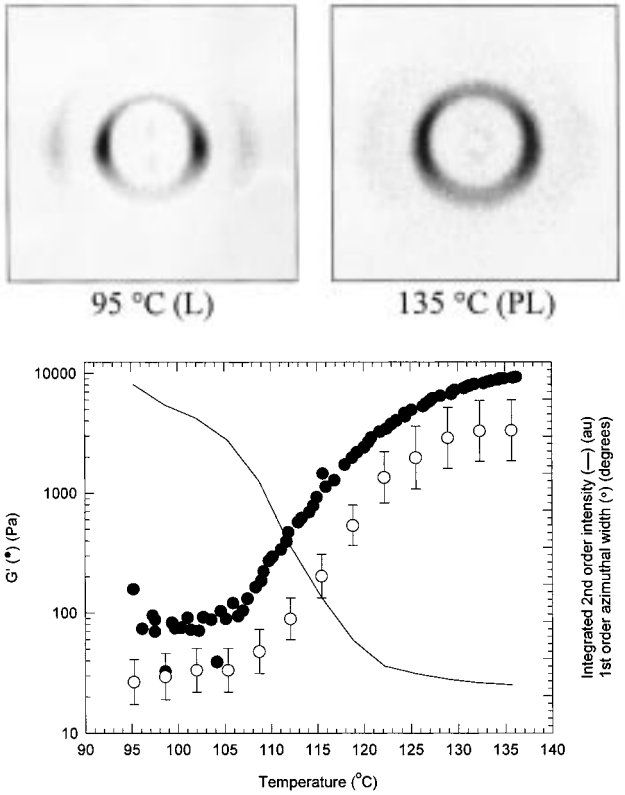

Figure 2. Scattering and rheological data for a shear-oriented PEO−PEE copolymer (OE−10; $f_{PEO} = 0.72$; oriented at $\omega = 100$ rad/s, $\gamma = 300\%$) heated through the L → PL transition. (top) SANS images recorded at 95 and 135 °C. The shear axis is vertical; the neutron beam is parallel to the shear gradient. At 95 °C, the system displays two well-oriented reflections characteristic of a lamellar phase at a radial position ratio of 1:2. Heating to 135 °C produces an increase in the azimuthal width of both reflections and a decrease in the intensity of the second-order peak. (bottom) Data recorded during a temperature ramp from 95 to 135 °C at 1 °C/min. The decline in the integrated intensity of the second-order reflection (—) and the increase in the azimuthal width of the first-order peak (○) coincides with the rise in elastic modulus (●) at $\omega = 1$ rad/s, $\gamma = 1\%$, which has been shown to indicate the L → PL transition.

by exposure to OsO_4 vapors and appear dark in the micrographs; polystyrene (majority component) domains appear relatively light.

Results

SANS measurements from shear-oriented lamellar phases generally show two azimuthally sharp reflections at radial position ratios of 1:2, consistent with a highly aligned layered morphology (Figure 2). Heating such morphologies across the L−G boundary, which is the lower limit of the temperature range within which the nonequilibrium PL structure is observed, produces a loss of layer orientation as evidenced by an increase in the azimuthal width of the first-order peak. At the same time, the radial width of the second-order reflection increases markedly, while the integrated intensity of this peak decreases. This suggests either a loss of long-range order within the lattice or a change in the form factor of the unit cell. Simultaneous rheological measurements (at $\gamma' = 1\%$, $\omega = 1$ rad/s) indicate that this behavior coincides with a sharp increase in the elastic modulus (G') of the specimen. SAXS measurements from shear-oriented materials show essentially identical structural changes: upon heating across the L−G boundary, reflections associated with the original lamellar phase gradually decline in intensity and eventually disappear, while a second set of peaks characteristic of a poorly ordered lamellar structure emerge and eventually reach a maximum value.

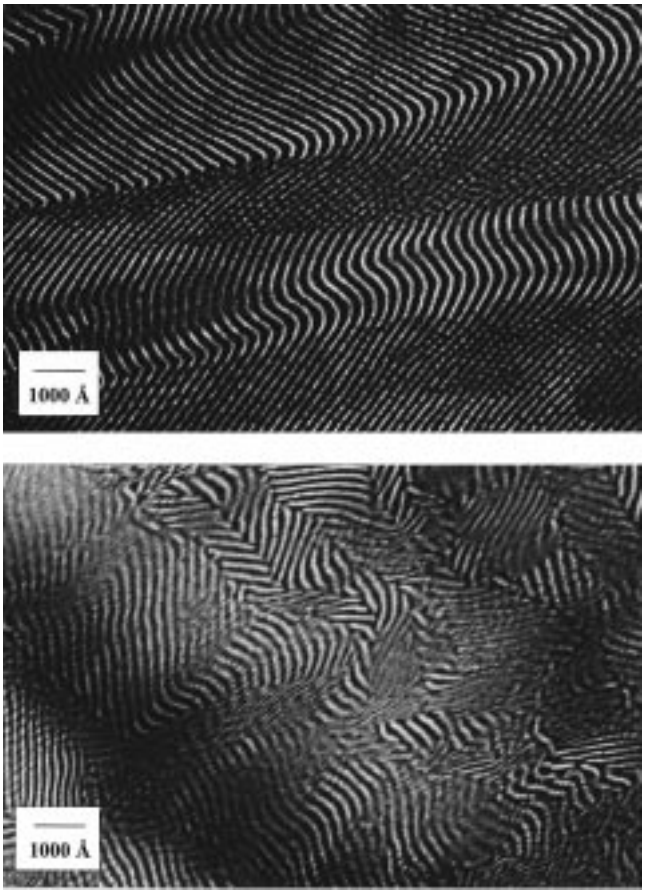

Figure 3. Electron micrographs of two PS−PI copolymers that were shear-oriented in the L phase, heated without shear into the PL phase, and then quenched in ice water. PI domains are stained with OsO_4 and appear dark. Top: IS-66 ($f_I = 0.66$), quenched after annealing for 5 min at 190 °C. Coexisting L and PL domains are observed; grain boundaries suggest that the PL domains grow through a peristaltic mechanism. Bottom: IS-65 ($f_I = 0.65$), quenched after annealing for 1 h at 200 °C. Relatively small domains of poorly ordered lamellae coexist with a second layered structure. The latter shows the periodic variation in minority layer contrast characteristic of perforated layers (PL).

Electron microscopy of samples quenched midway through the L → PL transition show coexisting lamellar and perforated layer domains, suggesting that the transformation proceeds through nucleation and growth of the PL structure (Figure 3). In the latter domains, neither an in-plane nor an out-of-plane ordering can be associated with the majority component channels, in agreement with the layerlike diffraction seen in both SAXS and SANS measurements. At grain boundaries separating the two morphologies, the layers exhibit notable variation in minority component layer thickness. This variation increases in amplitude upon crossing the boundary from the L to the PL edge. This suggests that the PL structure forms through the development of periodic distortions in the interface separating the blocks, which grow in amplitude until channels extending through the minority component domains are produced (Figure 4).[39,40] Such a "peristaltic mechanism" has been proposed for thermodynamically unstable lamellar phases.[17,39] Although distortions in adjacent layers will be correlated to some degree due to the incompressibility of the system and the resulting transmission of stresses along the layer normals, the lack of long-range order between the channels of the PL phase suggest that this coupling is relatively weak.

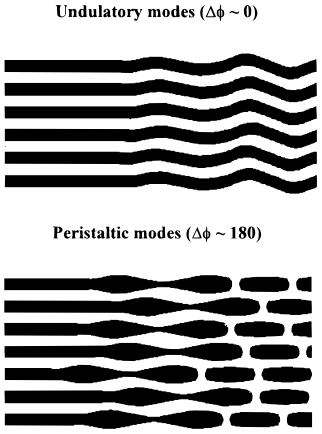

Figure 4. Undulatory and peristaltic deformation modes for a nonequilibrium lamellar structure. Minority component domains appear in black. Depending on the phase shift ($\Delta\phi$) between interfacial fluctuations on either side of a lamella, either peristaltic or undulatory modes may be produced. Electron microscopy provides direct evidence for the existence of the former and indirectly suggests the presence of the latter, although (as detailed in the text) the argument is by no means conclusive.

The lattice spacings of coexisting L and PL structures differ by an amount that depends on both the minority component volume fraction (f) and the conformational asymmetry (ϵ)[41] of the blocks, in agreement with theory [42] (Figure 5). For typical materials, $d_{PL} \sim 0.92d_L$. Given the coincidence in mean azimuthal orientation seen in the scattering measurements, this mismatch in lattice spacing could be accommodated through the formation of a tilt grain boundary at an angle of approximately $\cos^{-1} 0.92 = 22°$. Unfortunately, tilt angles measured from electron micrographs are typically about half of this value, which in turn suggests that the repeat spacing of both morphologies at the domain boundary are slightly distorted from that in the grain interior.

The transition mechanism depends to some degree on the composition of the sample. Rheological studies of G-forming diblocks with nearly identical molecular weights but slightly greater minority component fractions show a discontinuity in the slope of $G'(T)$ prior to forming the cubic phase.[30] Micrographs of shear-oriented samples that were quenched after annealing at temperatures where this rheological response is observed exhibit a microstructure consisting primarily of poorly ordered lamellae coexisting with small regions of the PL morphology (Figure 3). Although the former structure might result from interfacial distortions that are closely matched in phase (Figure 4), it is unlikely that such a small change in the composition of the system could produce such a dramatic shift in the character of the fluctuation modes. Another possibility is that the aforementioned mismatch in the L and PL spacings leads to the buckling of the layers, resulting in the poorly ordered morphologies shown in the micrographs. However, buckling is not seen in materials with slightly greater compositional asymmetries that exhibit similar disparities in spacing (Figure 2). At present, we do not have a satisfactory explanation for this behavior. The relatively small change in the viscoelastic response of the material at the transition presumably reflects the continued presence of the original lamellar phase.

Extended isothermal annealing of the PL structure does not produce long-range hexagonal order prior to the formation of the gyroid (G) morphology. Electron micrographs of shear-oriented samples quenched in liquid nitrogen after the initial stages of the PL → G relaxation show coexisting PL and G domains. Identification of the PL morphology is complicated

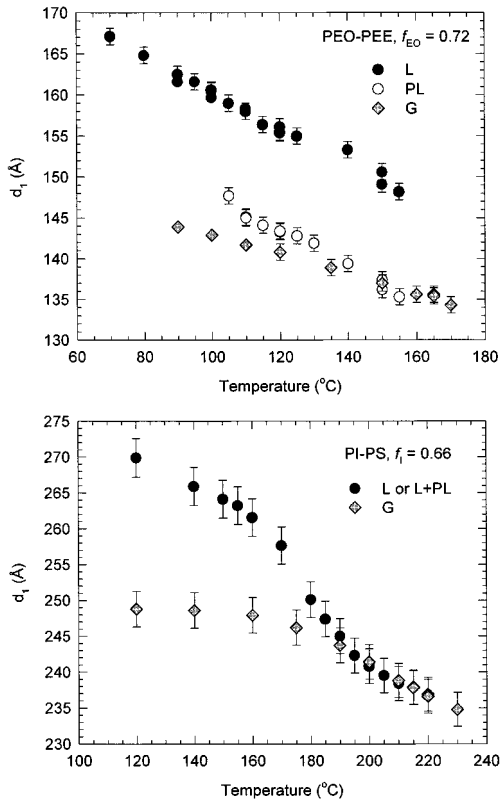

Figure 5. Equilibrium spacings of the L [10], PL [10], and G[211] lattice planes as a function of temperature for a PEO−PEE copolymer (OE-10, $f_{EO} = 0.72$) and the corresponding PI−PS material (IS-66, $f_I = 0.66$). The equilibrium nature of these spacings was confirmed by comparing values recorded upon heating and cooling; the slow kinetics of the PL → G relaxation permit us to identify an "equilibrium" spacing for the nonequilibrium PL phase. In the PI−PS system, the limited spatial resolution of the SAXS instrument precludes separation of the first-order peaks associated with the L and PL lattices. However, splittings in the higher order reflections confirm the presence of two coexisting lattices with different spacings, with $d_{PL} \sim 0.94d_L$, and the measured values depart from the linear dependence observed at low temperatures at the point where the L → PL transition is observed through rheology and TEM.

by the similarities between the (epitaxially related) edge view of the PL structure and the [211] and [221] projections of the G morphology for sections one unit cell in thickness.[43] Images from samples cooled on the rheometer after the initial stages of G phase formation (identified by an increase in $G'(T)$, the elastic shear modulus) show coexisting L and G domains (Figure 6); the appearance of the lamellar phase reflects the ease with which PL can return to L upon insufficiently rapid cooling. These coexisting domains are often separated by a narrow boundary region, several lamellar spacings in width, that consists of a poorly ordered morphology without any discernible long-range order. (The presence of epitaxial relations between the two phases shows that some order must be present, however).

Measurements of the PL and G spacings as a function of temperature reveal that rapid conversion of the PL structure, as evidenced by a sharp increase in the elastic modulus,[30] occurs only at temperatures where the PL [10] and G [211] spacings are nearly identical [37] (Figure 5); at temperatures where the spacings differ, formation of the equilibrium structure requires considerable annealing time. This frequently results in the development of large G phase monodomains, giving the diffraction produced by the cubic phase a "spotty" appearance (such as in Figure 4b of ref 22). This might reflect a nucleation-limited transition from PL to G or a rapid annealing process

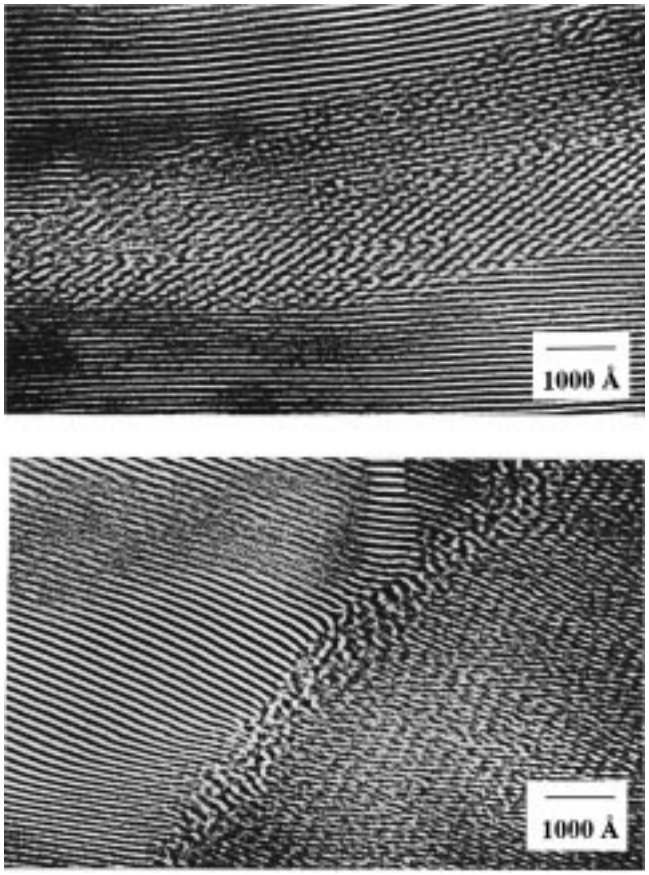

Figure 6. Electron micrograph from a PS−PI copolymer (IS-66, $f_i = 0.66$) that was shear-oriented in the PL phase at 190 °C, heated at 1 °C/min to 225 °C to induce the formation of the G phase, and then cooled to 20 °C. The presence of the L phase presumably results from slow cooling of the PL morphology (~1 °C/s) through temperatures at which the L phase is stable. PI domains are stained with OsO_4 and appear dark. (top) Coexisting L [10] and G [210] projections. (bottom) Coexisting L [10] and G [211] projections. In this case, the structures are separated by a relatively wide, poorly ordered region.

due to the highly symmetric nature of the cubic structure. In the former case, nucleation is presumably suppressed by the strain associated with the spacing mismatch at the PL−G grain boundaries.

Cooling the G phase returns samples to the L morphology without generating the PL structure. Previously published micrographs of G phase materials annealed at temperatures where the L phase is stable show coexisting L and G domains,[22] suggesting that this transformation also proceeds through nucleation and growth. The slow kinetics observed in rheological and scattering experiments are consistent with this view.

The spontaneous formation of large G phase monodomains can be used to identify the epitaxy associated with this transition. Figure 7 shows small-angle scattering images obtained from a G-forming copolymer upon rapid thermal quenching below the L−G phase boundary. As in the PL → G relaxation, the G [211] and L [10] lattice spacings coincide in azimuthal orientation, although they differ significantly in spacing. Samples quenched to temperatures relatively close to this boundary form only a single lamellar orientation, as evidenced by arcs at radial position ratios of 1:2. Samples quenched to lower temperatures frequently nucleate multiple lamellar orientations along the different [211] directions of the cubic unit cell (Figure 8). This occasionally produces images reminiscent of the HPL morphology due to the 6-fold rotational symmetry exhibited by the [211] lattice planes when viewed along the [111] axis. However,

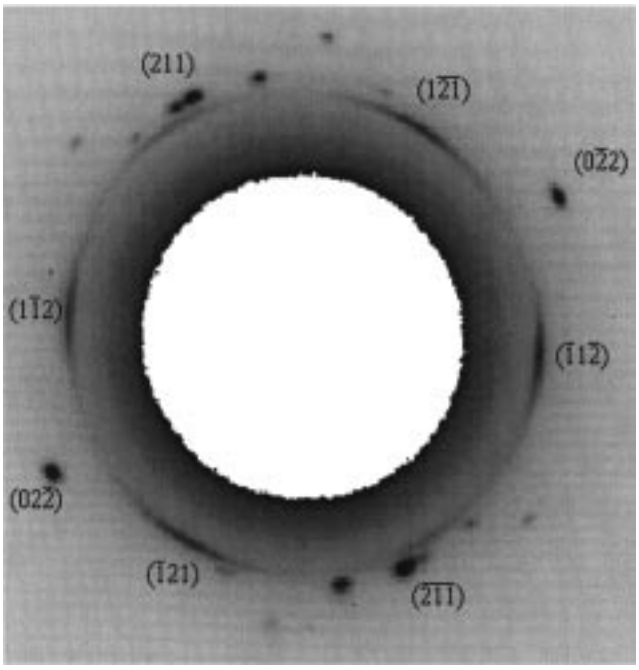

Figure 7. Small-angle diffraction from a PEP−PDMS copolymer (PEP−PDMS 7, $f_{PEP} = 0.65$) quenched from 174 to 50 °C. White and black denote regions of low and high intensity, respectively. The L → G transition occurs upon heating above 100 °C. Annealing at high temperatures in the absence of shear produces a relatively small number of highly oriented cubic phase domains. These generate the dark spots shown in this image; reflections from several different monodomains are visible. Rapid quenching below 100 °C results in the appearance of arcs at azimuthal positions associated with the different [211] axes of the cubic unit cells; reflections associated with one such orientation can be indexed as shown. Higher orders (not shown) appear at radial position ratios of 1:2, suggestive of a lamellar morphology.

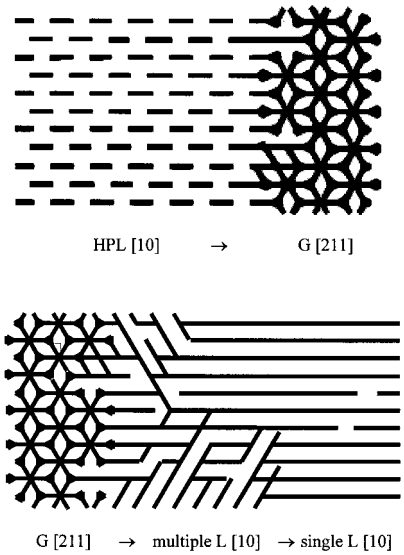

Figure 8. Schematic of the epitaxial relations involved in the (H)PL → G and G → L transformations. The G phase is shown along the [111] axis; other projections consistent with the appropriate epitaxial relations, such as [210] and [221], are commonly observed as well. Minority component domains are shown in black.

images from the quenched samples exhibit higher order reflections at radial position ratios of 1:2, whereas shear-oriented HPL phases generally fail to exhibit higher order reflections when viewed along the same orientation. The resulting epitaxy—G [211] → L [10]—complements that previously identified from

SANS measurements of the reverse transition—L [10] → HPL [10] → G [211].[20,21] The absence of such correlations from weakly sheared PL morphologies (consisting of highly oriented layers without a hexagonal ordering to the perforations) presumably reflects the rotational degeneracy of this structure about the [10] direction. The considerable difference in G [211] and L [10] spacings at the L−G phase boundary suggests that lamellar phase nucleation is suppressed in part by the considerable strain associated with L−G grain boundaries. We will return to this point below.

Discussion

The results presented here, together with conclusions drawn from a previous report [30] and recent theory,[12−17,44] lead us to conclude that the PL phase is a nonequilibrium structure in diblock copolymer melts. Here, we account for the appearance of this morphology by considering the implications of the microphase-separated interface for nucleation and growth phenomena. In part, the inspiration for this approach comes from previous studies of structurally homologous transitions in nonionic surfactants.[31−34]

During a transformation that proceeds via this mechanism, droplets of the final state form spontaneously within the initial structure and grow to encompass the entire sample volume. In the language of classical nucleation theory, the change in free energy upon forming a droplet of radius R is given by

$$\Delta F = 4\pi R^2\sigma + \frac{4\pi}{3}R^3(f_{new} - f_{old}) \quad (1)$$

where f_{new} and f_{old} are the free energy densities of the new and old phases, respectively, and σ is the surface energy associated with old phase−new phase grain boundaries. This change is maximized at a critical radius R_c, given by

$$R_c = \frac{2\sigma}{(f_{old} - f_{new})} \quad (2)$$

for which the associated increases in free energy is

$$\Delta F(R_c) = \frac{16\pi\sigma^3}{3(f_{old} - f_{new})^2} \quad (3)$$

Nuclei with $R > R_c$ are stable with respect to the old phase; $\Delta F(R_c)$ therefore represents the barrier to nucleation. This barrier can be crossed at a rate J_{nuc}, given by

$$J_{nuc} = \omega(R_c)\exp[-\Delta F(R_c)/kT] \quad (4)$$

where $\omega(R_c)$ is the frequency of attempts to form a droplet of radius R_c through thermal fluctuations.

The presence of a microphase-separated interface can strongly influence the kinetics of this process. First, generation of a structure with a different local topological genus necessarily involves tearing and re-forming the interface separating the blocks. The high energetic cost associated with such deformations implies that such events will be relatively infrequent in strongly segregated materials; that is, $\omega(R_c)$ will be low. Such suppression has been proposed to explain the kinetically hindered nature of bicontinuous phase formation in phospholipid suspensions.[33,34]

Second, once a region with the proper topological characteristics has been generated, maintaining interfacial continuity across a grain boundary that separates the initial and final morphologies will almost certainly involve considerable local distortion of both mesophases. The surface tension (σ) associated with such an interface will be relatively high, implying that newly formed final phase nuclei will therefore be stable only above an unusually large critical radius.[31,32] Thermal fluctuations that can produce such large nuclei may be relatively infrequent, and the rate of nucleation (J_{nuc}) will be correspondingly low. The sensitivity of the PL → G transition kinetics to the difference in spacing between the PL [10] and G [211] lattice planes, and the slow kinetics associated with the G → L transition, presumably reflect a strain-dependent contribution to this surface energy as well.

The second difficulty can be avoided by first transforming to a nonequilibrium structure with a more favorable local topology. Elsewhere, we have noted similarities between the commonly accepted models for the G phase and the HPL structure with an *abab*... interlayer stacking.[20,30,44] Both morphologies can be constructed from nearly identical, planar, 3-fold-coordinated minority component structural elements. In the G phase, successive elements are related through a rotation of 70.46° about the center of each minority component channel. In the HPL structure, the elements form a planar array of two-dimensional honeycomb lattices. That is, the HPL structure combines the local structure of the G phase with the overall symmetry of the initial L morphology. This permits it to form relatively low-angle (and hence low-energy) grain boundaries with the initial phase while simultaneously relieving most of the difference in free energy driving the L → G transition. Similar arguments have been used to explain the transient appearance of the C morphology during the L → G transformation in surfactant suspensions.[31,32]

We believe that differences in the nucleation rates associated with transitions between the L, PL, and G morphologies generate the sequence of ordered structures explored in this work. Figure 10 summarizes the relationships between the free energies of these structures as a function of temperature. As discussed above, we anticipate that the surface tension (σ) of L−PL boundaries is less than that of L−G boundaries. Since the free energies of the PL and G morphologies are nearly equal, the nucleation barrier (eq 3) for L → PL is less than that for L → G, resulting in the kinetically favored relaxation of metastable L phases to the PL morphology. Once the PL structure has formed, we expect that the free energy of PL−G grain boundaries will be comparable to that of L−G boundaries due to the layered structure of the L and PL morphologies. The (apparent) absence of direct L−G transitions suggests that both surface tensions are relatively large. Furthermore, the reduction in free energy obtained upon forming G within PL will be small. The PL → G relaxation will therefore have a large critical radius and a high barrier to nucleation (see eqs 2 and 3), resulting in slow relaxation kinetics. Such a nucleation-limited mechanism is consistent with the spontaneous appearance of highly ordered cubic monodomains upon annealing the PL state.

Evidence supporting this analysis comes from materials cycled between the L and G phases. Figure 9 displays a sequence recorded from a poly(ethylene oxide)−poly(ethylethylene) copolymer upon repeated thermal cycling. Heating the initial L phase produces a transformation to the PL structure; subsequent heating or extended isothermal annealing results in formation of the G phase. Cooling the G phase returns the sample to the L morphology, as expected. This is a slow transition, and so brief annealing (5 min) at low temperatures produces coexisting L and G domains. In rheological experiments, the response of this mixed morphology is apparently dominated by the high elastic modulus associated with the G

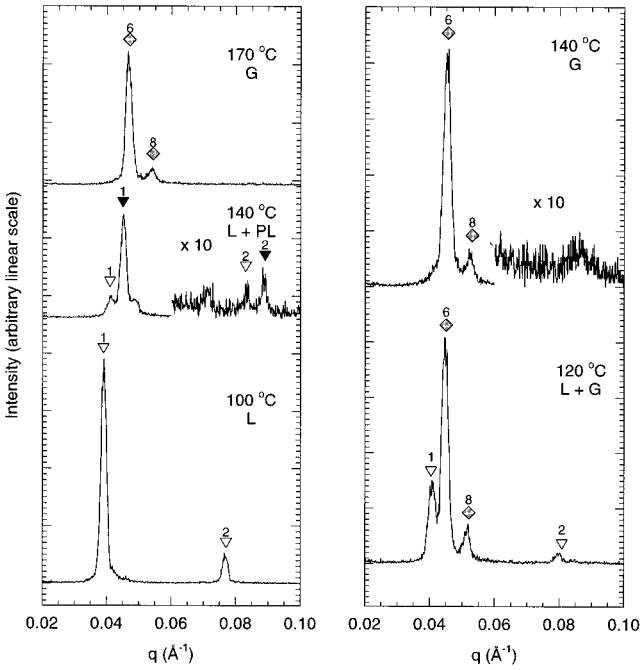

Figure 9. Grain boundary effects on transition mechanisms in a PEO−PEE copolymer (OE-10, $f_{EO} = 0.72$). L and PL peaks are marked by open and filled triangles; low-order G phase reflections are indicated by diamonds. The unmarked peaks associated with the PL channel packing appear at spacing ratios of $\sqrt{1}:\sqrt{2}$, suggesting a tetragonal arrangement characteristic of "bcc-based PL". (Left) Heating from 100, through 140, to 170 °C produces a transformation from L, to coexisting L and PL structures, and to the G morphology. (Right) Cooling the G morphology to temperatures at which L was initially observed returns the sample to the L phase; diffraction recorded immediately after cooling reveals coexisting L and G phases. Heating this mixed morphology to 140 °C produces a rapid L → G transition *without the appearance of the PL structure*, in contrast to results obtained when starting from a purely lamellar morphology. Direct L → G transitions are kinetically accessible once the mean size of the G domains exceeds a certain size.

phase.[37] Subsequent heating of the sample into the region where the PL phase was previously observed results in the growth of the G phase at the expense of the L domains. No diffraction associated with the PL state is observed. Contrary to our previous assertion,[37] it appears that direct transitions from L to G can occur in PL-forming systems once the mean size of the G domains exceeds a certain critical size.

The same considerations should govern the G → L transition as well. As in the L → G case, the high surface tension associated with L−G grain boundaries will severely restrict nucleation of the final morphology. Here, however, there does not appear to be an intermediate structure capable of forming low-energy grain boundaries with the cubic phase. As a result, a slow but direct transition from G to L is observed. Prior work has shown that the transition kinetics depend on the composition of the system;[30] this might reflect a compositional dependence on the magnitude of the epitaxially induced strain, and hence to the grain surface tension in the vicinity of the L−G phase boundary.

While the data presented here suggest that all three of the microstructural relaxations (L → PL, PL → G, and G → L) proceed through nucleation and growth following a shallow quench, it is certainly possible that thermodynamically unstable states could be prepared through rapid quenching. This is especially likely to occur in rheological studies involving the PL → G transition, where typical temperature ramp rates (∼1 °C/min) are much greater than the characteristic time scales for order−order transitions seen in isothermal annealing experiments

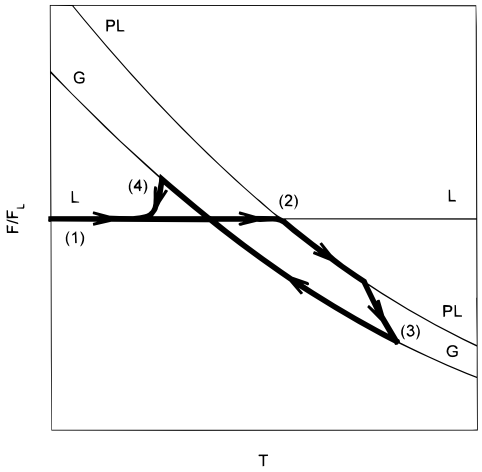

Figure 10. Schematic representation of the free energies for the L, PL, and G morphologies (in units of the lamellar phase free energy) as a function of temperature. The dark line traces the evolution of the system. Starting from low temperatures (1), the lamellar phase can be superheated above the L−G phase boundary into the region where the PL phase has a lower free energy. As argued in the text, direct L → G transitions are suppressed in favor of L → PL transitions by the difference in the associated nucleation rates, resulting in the formation of the PL phase (2). Extended annealing eventually results in the appearance of the equilibrium G morphology (3). The location of this transition shifts to lower temperatures upon reducing the temperature scan rate. Cooling the G phase below the L−G boundary returns the system to the original L morphology (4). The vertical and horizontal differences between these curves have been exaggerated for clarity; rheological data suggest that the L → PL and G → L temperatures coincide to within experimental resolution.

(∼hours).[30] Of course, in the absence of an unambiguous experimental signature for an "instability" mechanism, it will be difficult to differentiate such behavior from that associated with kinetic limits to nucleation and growth.[45,46]

Recent theoretical calculations have described mechanisms for the microstructural evolution of thermodynamically unstable initial states.[12−17] These include epitaxial relations between initial, intermediate, and final structures that are in excellent agreement with experiment.[18−21] Although such findings are not directly applicable to the experimental situation in view of the data presented here, we note that both the relaxation of an unstable morphology and the development of heterophase fluctuations within a metastable morphology are governed by the local slope of the free energy as a function of the appropriate order parameter. These epitaxies, then, might describe relative orientations of the two phases for which the probability of fluctuation-induced interfacial disruption is relatively high. Such disruption is required for nucleation of the final phase. In addition, they might also identify orientations that minimize the surface energy (σ) of the final phase domain; the existence of such an orientational dependence is implied by the highly elongated domain shape observed in electron micrographs. We anticipate that both effects are significant in these systems; a more quantitative statement is not possible in the absence of estimates for the grain surface energies of coexisting morphologies.

Conclusions

Order−order transitions between the lamellar (L), perforated layer (PL), and gyroid (G) phases proceed through nucleation and growth. Maintaining the continuity of microphase-separated interfaces across the resulting grain boundaries involves considerable local distortion of both morphologies. This arises from

differences in the geometrical characteristics of the phases and from mismatches in the spacings of epitaxially related lattice planes. The resulting strain raises the surface energy of the grains, severely restricting nucleation. Direct transitions from the lamellar to the gyroid phase are suppressed by this effect. Similar considerations have been identified in studies of the homologous transitions in aqueous surfactant suspensions.

Theoretical models for the evolution of thermodynamically unstable morphologies predict interfacial fluctuation modes, and epitaxial relations connecting initial and final morphologies, that are in excellent agreement with experiment. Since the interfacial disruption produced by such fluctuations is the first step in nucleation, this agreement suggests that the experimentally observed epitaxies describe relative orientations of the initial and final states for which the probability of such disruption—in other words, the frequency of nucleation attempts—is especially high. The presence of elliptical grains shows that there is an orientational dependence on the grain surface energy, which would also affect the distribution of nuclear alignments. Assessing the relative importance of these two contributions requires estimates for the free energy of these grain boundaries, which exist for the lamellar morphology[47−51] but are at present unavailable for coexisting mesophases.

Acknowledgment. We thank Dvora Perahia, Sol M. Gruner, and Jerry Hastings for assistance with the diffraction shown in Figure 7 and Zhen-Gang Wang for useful discussions. Support for this work was provided by the National Science Foundation (DMR-9405101), the Air Force Office of Scientific Research (AF/F49620-96), and the Danish Polymer Center, a Research Center at Risø National Laboratory and the Danish Technical University sponsored by the Programme for Development of Materials Technology.

References and Notes

(1) Bates, F. S.; Schulz, M. F.; Khandpur, A. K.; Förster, S.; Rosedale, J. H.; Almdal, K. A.; Mortensen, K. *Faraday Discuss.* **1994**, *98*, 7 and references therein.
(2) Matsen, M. W.; Bates, F. S. *Macromolecules* **1996**, *29*, 1091, and references therein.
(3) Helfand, E. *Macromolecules* **1975**, *8*, 552.
(4) Helfand, E.; Wasserman, Z. R. *Macromolecules* **1976**, *9*, 879.
(5) Helfand, E.; Wasserman, Z. R. *Macromolecules* **1978**, *11*, 960.
(6) Helfand, E.; Wasserman, Z. R. *Macromolecules* **1980**, *13*, 994.
(7) Semenov, A. N. *Sov. Phys. JETP* **1985**, *61*, 733.
(8) Vavasour, J. D.; Whitmore, M. D. *Macromolecules* **1992**, *25*, 5477.
(9) Hasegawa, H.; Tanaka, H.; Yamasaki, K.; Hashimoto, T. *Macromolecules* **1987**, *20*, 1651.
(10) Thomas, E. L.; Alward, D. B.; Kinning, D. J.; Martin, D. C.; Handlin, D. L.; Fetters, L. J. *Macromolecules* **1986**, *19*, 2197.
(11) Sakurai, S.; Momii, T.; Taie, K.; Shibayama, M.; Nomura, S.; Hashimoto, T. *Macromolecules* **1993**, *26*, 485.
(12) Qi, S.; Wang, Z.-G. *Phys. Rev. Lett.* **1996**, *76*, 1679.
(13) Qi, S.; Wang, Z.-G. *Phys. Rev. E* **1997**, *55*, 1682.
(14) Qi, S.; Wang, Z.-G. *Macromolecules* **1997**, *30*, 4491.
(15) Shi, A.-C.; Noolandi, J.; Desai, R. C. *Macromolecules* **1996**, *29*, 6487.
(16) Laradji, M.; Shi, A.-C.; Desai, R. C.; Noolandi, J. *Phys. Rev. Lett.* **1997**, 78, 2577.
(17) Laradji, M.; Shi, A.-C.; Noolandi, J.; Desai, R. C. *Macromolecules* **1997**, *30*, 3242.
(18) Sakurai, S.; Momii, T.; Taie, K.; Shibayama, M.; Nomura, S.; Hashimoto, T. *Macromolecules* **1993**, *26*, 485.
(19) Hajduk, D. A.; Gruner, S. M.; Rangarajan, P.; Register, R. A.; Fetters, L. J.; Honeker, C.; Albalak, R. J.; Thomas, E. L. *Macromolecules* **1994**, *27*, 490.
(20) Förster, S.; Khandpur, A. K.; Zhao, J.; Bates, F. S.; Hamley, I. W.; Ryan, A. J.; *Macromolecules* **1994**, *27*, 6922.
(21) Zhao, J.; Majumdar, B.; Schulz, M. F.; Bates, F. S.; Almdal, K.; Mortensen, K.; Hajduk, D. A.; Gruner, S. M. *Macromolecules* **1996**, *29*, 1204.
(22) Hajduk, D. A.; Harper, P. E.; Gruner, S. M.; Honeker, C. C.; Kim, G.; Thomas, E. L.; Fetters, L. J. *Macromolecules* **1994**, *27*, 4063.
(23) Goveas, J. L.; Milner, S. T. *Macromolecules* **1997**, *30*, 2605.
(24) Harkless, C. R.; Singh, M. A.; Nagler, S. E.; Stephenson, G. B.; Jordan-Sweet, J. L. *Phys. Rev. Lett.* **1990**, *64* (19), 2285.
(25) Singh, M. A.; Harkless, C. R.; Nagler, S. E.; Shannon, R. F.; Ghosh, S. S. *Phys. Rev. B* **1993**, *47* (14), 8425.
(26) Schuler, M.; Stühn, B. *Macromolecules* **1993**, *26*, 112.
(27) Stühn, B.; Vilesov, A.; Zachmann, H. G. *Macromolecules* **1994**, *27*, 3560.
(28) Hashimoto, T.; Sakamoto, N. *Macromolecules* **1995**, *28*, 4779.
(29) Hajduk, D. A.; Tepe, T.; Takenouchi, H.; Tirrell, M.; Bates, F. S.; Almdal, K.; Mortensen, K. *J. Chem. Phys.* **1998**, *108* (1), 326.
(30) Hajduk, D. A.; Takenouchi, H.; Hillmyer, M. A.; Bates, F. S.; Vigild, M. E.; Almdal, K. *Macromolecules* **1997**, *30*, 3788.
(31) Rançon, Y.; Charvolin, J. *J. Phys.* **1987**, *48*, 1067.
(32) Charvolin, J. *Contemp. Phys*. **1990**, *31*, 1.
(33) Shyamsunder, E.; Gruner, S. M.; Tate M. W.; Turner, D. C.; So, P. T. C. *Biochemistry* **1988**, *27*, 2332.
(34) Gruner, S. M. *J. Chem. Phys.* **1989**, *93*, 7562.
(35) Khandpur, A. K.; Forster, S.; Bates, F. S.; Hamley, I. W.; Ryan, A. J.; Bras, W.; Almdal, K.; Mortensen, K. *Macromolecules* **1995**, *28*, 8796.
(36) Almdal, K.; Mortensen, K.; Ryan, A. J.; Bates, F. S. *Macromolecules* **1996**, *29*, 5940.
(37) Hillmyer, M. A.; Bates, F. S.; Almdal, K.; Mortensen, K.; Ryan, A. J.; Fairclough, J. P. A. *Science* **1996**, *271*, 976.
(38) Hillmyer, M. A.; Bates, F. S. *Macromolecules* **1996**, *29*, 6994.
(39) Yeung, C.; Shi, A.-C.; Noolandi, J.; Desai, R. C. *Macromol. Theory Simul*. **1996**, *5*, 291.
(40) Hamley, I. W.; Koppi, K. A.; Rosedale, J. H.; Bates, F. S.; Almdal, K.; Mortensen, K. *Macromolecules* **1993**, *26*, 5959.
(41) Vavasour, J. D.; Whitmore, M. D. *Macromolecules* **1993**, *26*, 7070; *Macromolecules* **1996**, *29*, 697.
(42) Matsen, M. W.; Bates, F. S. *J. Polym. Sci. B.* **1996**, *35*, 945.
(43) Harper, P. E. Structural Studies of Surfactant and Polymer Systems. Ph.D. thesis, Princeton University, 1996.
(44) Matsen, M. W.; Bates, F. S. *Macromolecules* **1996**, *29*, 7641.
(45) Debenedetti, P. *Metastable Liquids: Concepts and Principles* Princeton University Press: Princeton, NJ, 1996.
(46) Fredrickson, G. H.; Binder, K. *J. Chem. Phys.* **1989**, *91*, 7265.
(47) Gido, S. P.; Gunther, J.; Thomas, E. L.; Hoffman, D. *Macromolecules* **1993**, *26*, 4506.
(48) Gido, S. P.; Thomas, E. L. *Macromolecules* **1994**, *27*, 849.
(49) Gido, S. P.; Thomas, E. L. *Macromolecules* **1994**, *27*, 6137.
(50) Gido, S. P.; Thomas, E. L. *Macromolecules* **1997**, *30*, 3739.
(51) Matsen, M. W. *J. Chem. Phys.* **1997**, *107*, 8110.